OPTICA

PUBLISHING GROUP

Formerly OSA

Resonant Cavity-Enhanced Photodiode Array for Miniaturised Spectroscopic Sensing

ANDREW BAINBRIDGE,[1,*] LAURA A. HANKS,[1] ADAM P. CRAIG,[1] AND ANDREW R. J. MARSHALL[1]

[1]*Physics Department, Lancaster University, Lancaster UK, LA1 4YB*
a.bainbridge@lancaster.ac.uk

Abstract: Optical spectroscopic sensing is a technique that is commonly employed for the identification and compositional analysis of a wide variety of substances, from biological samples to greenhouse gases. High-resolution spectrometers are well established, however, attempts to miniaturise the designs can suffer from adverse effects due to the miniaturisation, for both Fourier transform based interferometric designs, as well as dispersive designs. In this work a linear array of resonant cavity-enhanced photodiodes is realised with spatially chirped resonance wavelength, offering chip-scale free-space hyperspectral sensing. Resonant cavity-enhanced photodiodes sense over a narrow spectral band, which can be tuned by the thicknesses of the heterostructure. Through this work, multiple narrow spectral bands can be sensed by resonant cavity-enhanced photodiodes on a single chip by grading the thicknesses across the wafer. Photocurrent measurements from a fabricated array determine the wavelength of incident light with an accuracy of $\pm$ 2 nm.

1. Introduction

The miniaturisation of sensors capable of high-resolution spectroscopic measurements is of significant interest to countless applications where traditional, bulky spectrometers are not feasible. For example, continuous health monitoring can be undertaken by spectroscopic sensing, [1, 2] but small-size equipment is a significant requirement for real-world use. There have been many recent attempts to miniaturise spectrometers including interferometric designs, [3, 4] and dispersive designs, [5–13] however they can suffer from adverse effects due to the miniaturisation. A different approach is to utilise a photodetector with an intrinsic spatial variation in spectral response, thereby allowing an incident spectrum to be reconstructed through simultaneous measurements of pixels with varied spectral responses. This approach has been demonstrated previously, e.g. by Yang et al. [14] The photocurrent responses of multiple broadband detectors can be used to recreate an incident spectrum, however, significant data analysis of the measured outputs is required and discrimination of complex spectra is limited. The intrinsic narrow spectral response of resonant cavity-enhanced photodiodes (RCE-PDs) makes them ideal detectors for spectroscopic measurements at a single wavelength and also makes them ideal for spectrum recreation, if utilising multiple detectors. An array of RCE-PDs with varied spectral responses has a much reduced overlap of the responses between neighbouring pixels in comparison to broadband detectors and accurate hyperspectral sensing can be achieved without significant post-measurement analysis. This removes the risk of misinterpretation of the incident spectrum and offers a path to miniature high-resolution spectral sensing in simple free-space applications.

2. Methods

The RCE-PD linear array in this work, figure 1a, utilises a variation in thickness across one dimension of the chip to implement a corresponding variation, or 'chirp', in spectral response. The thickness gradient is achieved by pausing the rotation of the wafer during molecular beam
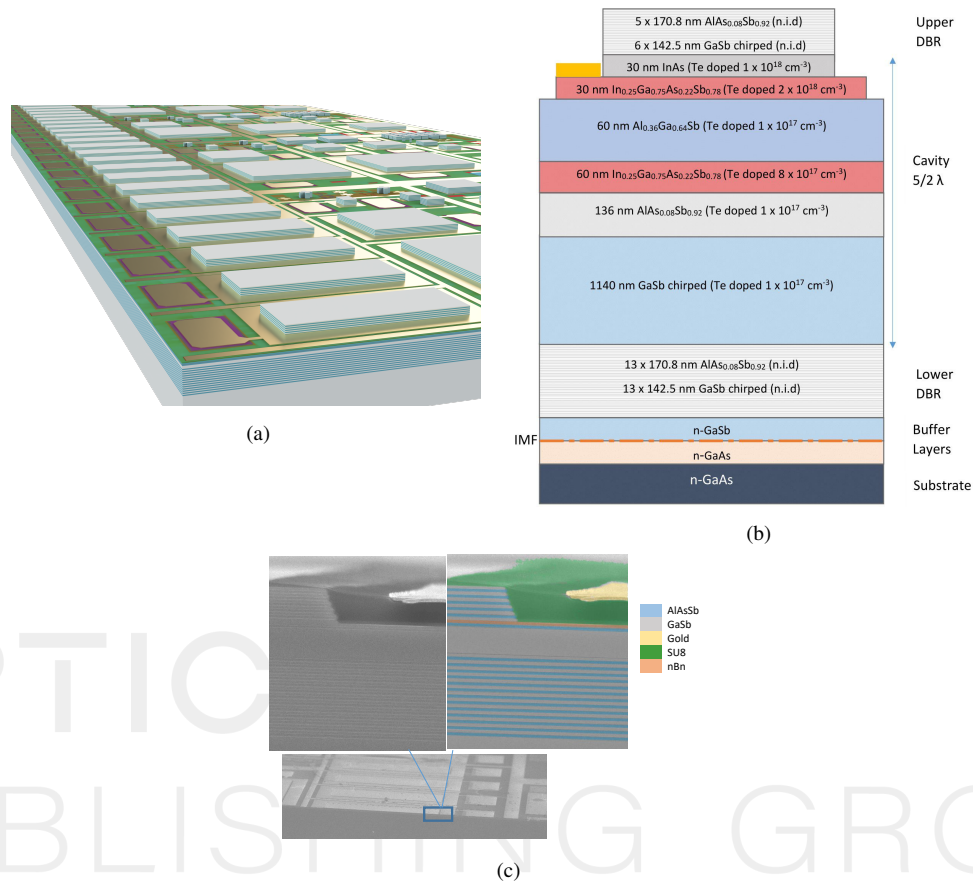
Fig. 1. a) 3D render of the final processed sample - thicknesses are enhanced by one order of magnitude for visualisation. b) Full epi-structure of the fabricated sample. c) SEM images of the fabricated sample, including cross-section with false colour to aid material identification.

epitaxy (MBE) growth of the structure, [15] so that there is a growth rate gradient across the wafer - based on the geometry of the growth chamber and source cells. With no rotation adsorption does not occur evenly across the sample - as is usually desired - and the growth rate exhibits a gradient along an axis from the group III cell. This technique was only used during the growth of binary materials to avoid introducing a composition gradient across the sample; which would be incompatible with lattice-matched growth. The growth rate gradient has been seen to be consistent across an extended period of time, so a simple calibration growth could allow repeatable mass production.

Aside from the wafer rotation, the growth process is equivalent to that for conventional RCE-PD structures. The concept of the chirped RCE-PD linear array could be employed with any DBR based RCE-PD structure. The results presented here utilise a structure extended from recent work on single-wavelength RCE-PDs sensing in the short-wave infrared. [16] Samples operating in the mid-wave infrared have also been developed (supplementary section 4). The structure, figure 1b, denotes a specific, nominal thickness for the layers, although the thicknesses of certain layers, namely the GaSb layers, are graded in one-dimension across the wafer. The impact of the thickness variations on the spectral response can be understood by considering the electric field in the structure. For the nominal thicknesses specified in the design, the electric field interferes
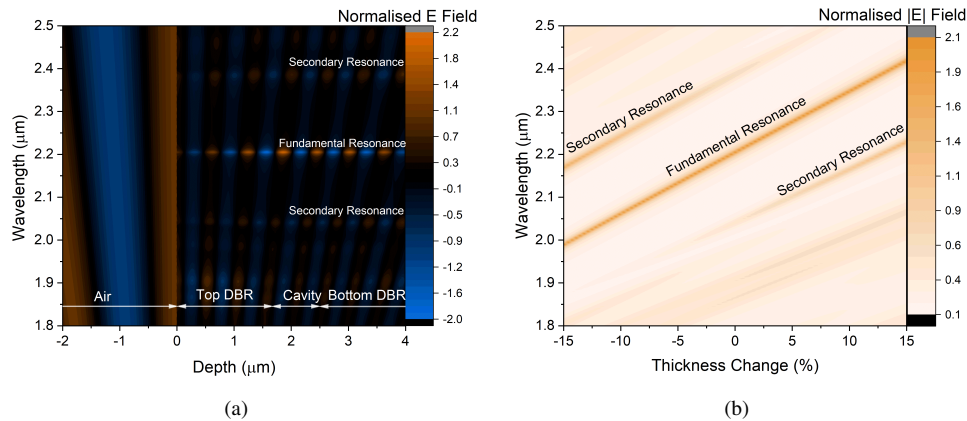
Fig. 2. a) Modelled electric field in the structure for the nominal layer thicknesses. b) Modelled electric field enhancement factor in the absorber as a function of wavelength and change in layer thicknesses. The condition modelled is for the case where all GaSb layers in the structure are subject to the given thickness change.

constructively in the structure at 2.2 μm, figure 2a. There are also lower amplitude secondary resonances at wavelengths either side of the fundamental. As the thickness varies the wavelength for constructive interference of the electric field in the absorber also varies, seen as the maximum field strength in figure 2b. The wavelengths of the secondary resonances also shift simultaneously, and become more or less prominent due to the mismatch between the layer thicknesses.

The design of the fabricated wafer incorporates the thickness variation for the GaSb layer in the cavity and all the GaSb layers in the DBRs. The cavity is thicker to accommodate a 2λ binary layer with graded thickness to maximise the resonance shift. The concept would still work with a more conventional $1/2\lambda$ cavity, and without a reduction in the resonance shift if thickness grading of complex alloys can be achieved. A 2-inch lattice-mismatched GaAs substrate was used instead of native GaSb for higher transparency in the target spectral region, facilitating study of the cavity by optical transmission, however the choice of substrate is not specific to the chirped RCE-PD concept.

An interfacial misfit array (IMF) [17] was utilised to allow for growth of subsequent layers lattice-matched to GaSb. An approximately 500 nm thick GaSb buffer layer was grown first after the IMF, followed by the structure. All layers were grown at approximately 1 ML/s. X-ray diffraction measurements were used to determine close lattice matching for the ternary layers (supplementary figure 1). Standard micro-lithography techniques were used to fabricate devices. The top DBR was etched to allow the contacts to be placed on the top InGaAsSb layer; device mesas were subsequently defined by etching this layer. Ti/Au bondpads were evaporated onto a SiN dielectric base; the same evaporation also created a metal mask over the mesa area not covered by the top DBR - isolated from the photodiodes by an SU-8 passivation layer. The metal mask ensures light can only enter the cavity and absorber through the DBR, to remove the undesirable broadband response seen by other RCE-PDs. [16, 18–21] For the purposes of testing the structure for hyperspectral sensing a linear array was created along the thickness gradient on the sample, figure 1a. Each rectangular pixel consisted of a light-sensitive area of 466 μm by 166 μm, with a pitch between pixels of 333 μm. To allow for complete optoelectronic characterisation of the sample multiple single element PCE-PDs of varying area were also created on the same sample.

3. Results and discussion

The spatial dependence of the resonance wavelength was characterised through transmission 2D mapping across the full wafer, directly after epitaxial growth, figure 3a shows the approximately one-dimensional variation of the resonance wavelength achieved across the sample. The measured spatial chirp coefficient is 14 nm/mm along the axis of thickness chirp. With reference to the modelled dependence this equates to a thickness variation of the GaSb epi-layers of $\sim 1\,\%\,\mathrm{mm}^{-1}$.

A 26 pixel detector array was fabricated from a portion of the wafer, with the approximate postion on the wafer highlighted in figure 3a. The resonance wavelengths of the pixels vary from 1984 nm to 2086 nm, equating to a shift of approximately 4 nm per pixel - figure 3b. The responses are approximately Gaussian in shape, with a FWHM of ~ 30 nm that does not vary significantly across the wafer. The peak quantum efficiency of each pixel is approximately the same; room-temperature values of around 55 % were measured. The pixels also have a signal-to-noise performance comparable to previously reported single-wavelength RCE-PDs (supplementary section 2).

The quantum efficiency for a representative pixel with an applied bias voltage of -500 mV is shown in figure 3c. There is a second lower resonance due to the choice of a thick, $5/2\lambda$, cavity - designed to accommodate a thick graded layer in the cavity. The thick cavity reduces the free spectral range between the fundamental and secondary peaks, which is inversely proportional to the optical path length of the cavity. Future designs can significantly reduce the secondary peaks by reducing the cavity thickness (supplementary section 4.1), with a cost of a slight reduction in the spatial chirp coefficient.

As a simple first demonstration of the high resolution spectral sensing possible with the linear array, the photocurrent generated by each pixel was measured under illumination from a monochromator. Gaussian fitting of the normalised photocurrents comfortably discriminates between each wavelength tested. Furthermore, using the known resonance wavelengths of the pixels the wavelength of the incident light can be interpreted with a precision of ± 2 nm, including monochromator uncertainty of ± 0.5 nm. It is likely more complex spectra could be reconstructed, with higher resolution, through analysis of the combined photocurrent measurements of all the pixels in the linear array, however, this letter is focused on the introduction of the novel RCE-PD array. Further optimisation of the structure can reduce the FWHM of the fundamental resonances and amplitude of secondary resonances (supplementary section 4). This can reduce the overlap of the spectral responses and increase the resolution and discrimination possible. Modelling indicates a resolution of 0.1 nm should be achievable using this approach, and enhanced data analysis could increase this further.

The spectral reconstruction is based on easily obtainable prior knowledge of the characteristic spectral response of each pixel, but no prior knowledge of the incident spectrum is assumed. For this method to be accurate the factors that influence the response of the pixels need to be understood. One factor is the temperature, which monotonically increases the FWHM and wavelength of the resonance. [16] However, the coefficients are small because they are defined principally by the temperature dependence of the refractive indices. [18] Measurements determine coefficients of ~ 0.17 nm/K for the shift of the peak wavelength - figure 4a - and ~ 0.04 nm/K for the FWHM; for comparison, the cutoff wavelength of the absorber material, outside a resonant cavity, shifts by ~ 1.4 nm/K. [16] These factors could be corrected based on a simple temperature measurement. The amplitude of the response also shifts with temperature - figure 4a - however, it is not a linear change. However, the relative response of the pixels should not vary with temperature and hence correction is unlikely to be required.

The angular dependence of the resonance wavelength is less well studied than the temperature dependence but does also need to be considered. Reflectance measurements on the wafer prior to processing - figure 4b - show that the resonance wavelength decreases as the angle of the incident light increases with respect to normal, by ~ 1.2 nm/$^\circ$. Any shift due to angle could be corrected
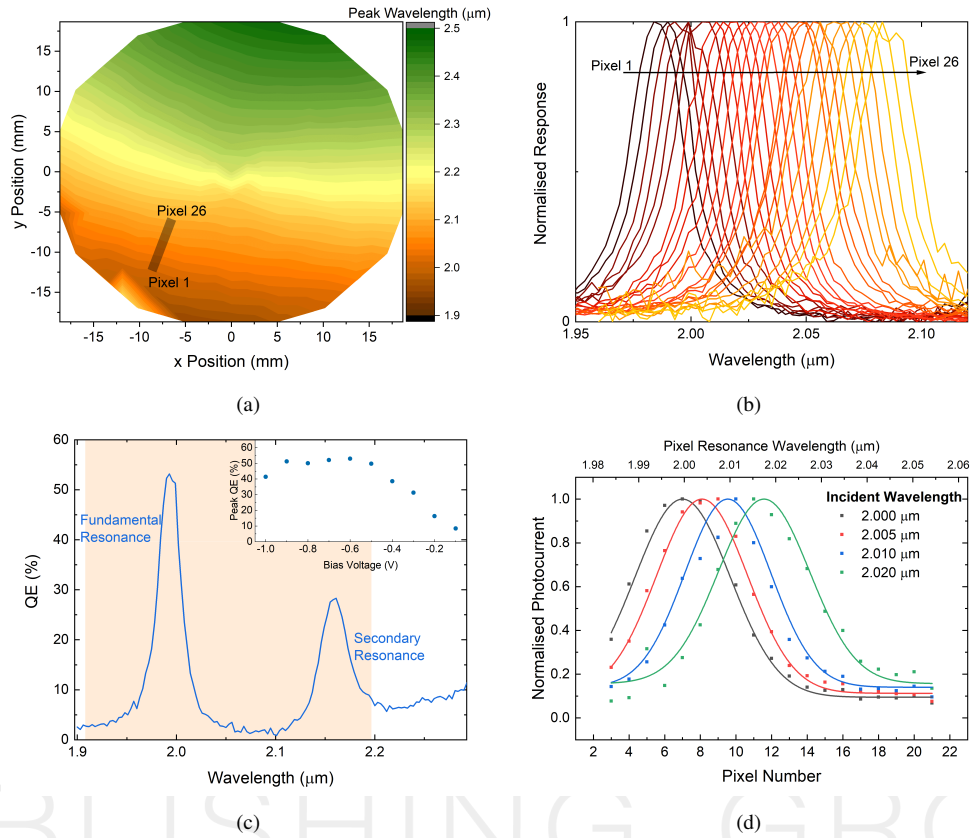
Fig. 3. a) Colour-map of the resonance wavelength determined from transmission measurements on the unprocessed wafer. b) Normalised spectral response curves of 26 consecutive pixels from an arbitrary piece of the sample - zoomed in on resonance. c) Quantum efficiency for a single pixel. Shaded area indicates the mirror stopband. Inset: bias voltage dependence of peak QE. d) The photocurrents of each pixel along a linear array under illumination from a monochromator.

based on knowledge of the focusing optics or minimised by reducing the angle of incidence.

The novel chirped RCE-PD linear array has been shown to comfortably discriminate between monochromator output spectra 5 nm apart and with further optimisation enhanced resolution and stability can be achieved. Variation of the number of DBR layers and the thickness of the absorber can increase the Q-factor of the cavity. Narrower widths would increase the spectral specificity of each pixel and increase the potential resolution - nanometre scale FWHMs are achievable in RCE devices [22]. Additionally, a reduction in the pixel pitch used here (see methods) could further increase the resolution.

The structure that has been fabricated only includes thickness grading of the binary GaSb layers, however, it would be possible to extend the grading to the entire structure - including the ternary AlAsSb alloy. Lattice matching across the entire substrate could be sufficiently maintained by mounting the As and Sb cells next to each other on the growth chamber, to reduce variations in the ratio of the two fluxes across the substrate. Implementation of the thickness grading of the entire structure would double the rate of the spectral chirp (supplementary figure 3) increasing the width of the spectral band covered by a linear array.

Integration of the linear array into small electronic devices would be straightforward. There is
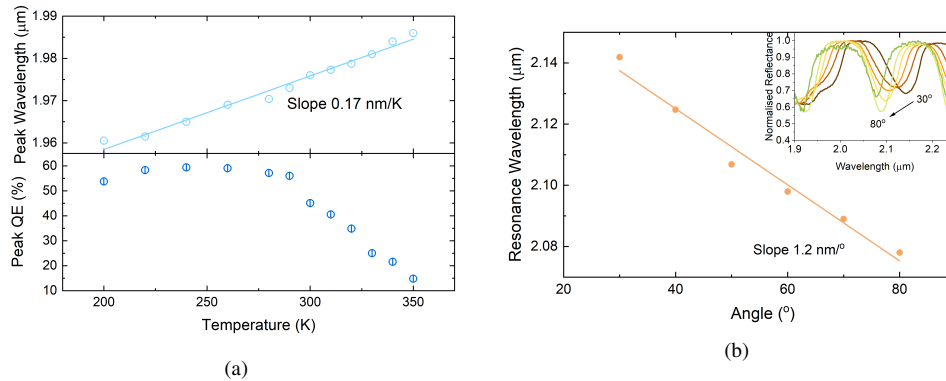
Fig. 4. a) Top: The temperature dependence of the fundamental resonance wavelength for a single pixel. Bottom: The temperature dependence of the peak quantum efficiency for a representative pixel. b) The angular dependence of the resonance wavelength, determined from reflectance measurements on the unprocessed wafer. Inset: The normalised reflectance curves from which the resonance wavelengths were extracted.

no requirement for significant additional components and the fabrication process is compatible with existing standard lithography techniques. Current high-end smartphone camera sensors are of the order of 10 mm side length; a similar length RCE-PD linear array would be able to cover a spectral band of ~ 140 nm, or ~ 270 nm if all the structure layers could be graded. The width of the linear array is negligible compared to the length, so it would also be simple to integrate multiple linear arrays next to each other without substantially increasing the required space. This would allow light from multiple spectral ranges to be measured simultaneously. One potential use is for blood glucose monitoring which can be measured by light in the short-wave infrared. Previous reports of optical in-vivo glucose monitoring have utilised lab spectrometers to demonstrate the feasibility of this method, [2] whereas discrete wavelength sensing has struggled to reliably detect glucose in-vivo. True spectral information from a chip scale sensor offers the possibility of taking lab demonstration into consumer applications. The RCE-PD linear array design could be designed for many other spectroscopic applications sensing at wavelengths from ultraviolet to long-wave infrared spectral ranges; DBR based RCE-PDs have previously been demonstrated at multiple significant wavelengths. [16, 18–21, 23–25]

4. Conclusion

A key promise of RCE-PDs has been spectroscopic sensing of individual absorption lines with high specificity - the chirped RCE-PD linear array presented significantly enhances the scope of this capability to the simultaneous discrimination of multiple absorption lines. Since pure substances are rare in many applications outside of the lab, the recreation of an entire band of the spectrum makes the device much more versatile, less affected by changing environmental backgrounds and not limited to measurement of a single substance. The discrimination of closely spaced single-wavelengths demonstrates the possibilities of the RCE-PD linear array, but it is expected the potential of the new platform will be unlocked by on-chip integration and further optimisation of both array and data processing towards specific applications.

Acknowledgments

Disclosures

The authors declare an interest in a patent application. UK number 2110690.1, by Lancaster University, for inventors: Andrew Marshall and Andrew Bainbridge, recently submitted. Aspect covered: the use of thickness variations across a wafer to chirp the spectral response of RCE-PDs. This allows for the hyperspectral sensing by pixels on the same chip.

Data availability

Data underlying the results presented in this paper are available in Ref. [26].

Supplemental document

See Supplement 1 for supporting content.

References

1. A. Currà, R. Gasbarrone, A. Cardillo, C. Trompetto, F. Fattapposta, F. Pierelli, P. Missori, G. Bonifazi, and S. Serranti, "Near-infrared spectroscopy as a tool for in vivo analysis of human muscles," Sci. Reports **9**, 8623 (2019).
2. M. A. Arnold, L. Liu, and J. T. Olesberg, "Selectivity assessment of noninvasive glucose measurements based on analysis of multivariate calibration vectors," J. Diabetes Sci. Technol. **1**, 454–462 (2007). PMID: 19885107.
3. P. Malara, A. Giorgini, S. Avino, V. Di Sarno, R. Aiello, P. Maddaloni, P. De Natale, and G. Gagliardi, "A self-operating broadband spectrometer on a droplet," Nat. Commun. **11**, 2263 (2020).
4. D. Knipp, H. Stiebig, S. R. Bhalotra, E. Bunte, H. L. Kung, and D. A. B. Miller, "Silicon-based micro-fourier spectrometer," IEEE Transactions on Electron Devices **52**, 419–426 (2005).
5. M. Faraji-Dana, E. Arbabi, A. Arbabi, S. M. Kamali, H. Kwon, and A. Faraon, "Compact folded metasurface spectrometer," Nat. Commun. **9**, 4196 (2018).
6. R. F. Wolffenbuttel, "State-of-the-art in integrated optical microspectrometers," IEEE Transactions on Instrumentation Meas. **53**, 197–202 (2004).
7. Y. Horie, A. Arbabi, E. Arbabi, S. M. Kamali, and A. Faraon, "Wide bandwidth and high resolution planar filter array based on dbr-metasurface-dbr structures," Opt. Express **24**, 11677–11682 (2016).
8. M. Kunitski, N. Eicke, P. Huber, J. Köhler, S. Zeller, J. Voigtsberger, N. Schlott, K. Henrichs, H. Sann, F. Trinter, L. P. H. Schmidt, A. Kalinin, M. S. Schöffler, T. Jahnke, M. Lein, and R. Dörner, "Double-slit photoelectron interference in strong-field ionization of the neon dimer," Nat. Commun. **10**, 1 (2019).
9. B. Redding, S. F. Liew, R. Sarma, and H. Cao, "Compact spectrometer based on a disordered photonic chip," Nat. Photonics **7**, 746–751 (2013).
10. N. K. Pervez, W. Cheng, Z. Jia, M. P. Cox, H. M. Edrees, and I. Kymissis, "Photonic crystal spectrometer," Opt. Express **18**, 8277–8285 (2010).
11. S.-W. Wang, C. Xia, X. Chen, W. Lu, M. Li, H. Wang, W. Zheng, and T. Zhang, "Concept of a high-resolution miniature spectrometer using an integrated filter array," Opt. Lett. **32**, 632–634 (2007).
12. B. Momeni, E. S. Hosseini, M. Askari, M. Soltani, and A. Adibi, "Integrated photonic crystal spectrometers for sensing applications," Opt. Commun. **282**, 3168–3171 (2009).
13. X. Gan, N. Pervez, I. Kymissis, F. Hatami, and D. Englund, "A high-resolution spectrometer based on a compact planar two dimensional photonic crystal cavity array," Appl. Phys. Lett. **100**, 231104 (2012).
14. Z. Yang, T. Albrow-Owen, H. Cui, J. Alexander-Webber, F. Gu, X. Wang, T.-C. Wu, M. Zhuge, C. Williams, P. Wang, A. V. Zayats, W. Cai, L. Dai, S. Hofmann, M. Overend, L. Tong, Q. Yang, Z. Sun, and T. Hasan, "Single-nanowire spectrometers," Science **365**, 1017–1020 (2019).
15. University of Lancaster, "Resonant cavity enhanced photodetectors," (2021). UK Patent Application No. 2110690.1.
16. A. Bainbridge, K. Mamic, L. A. Hanks, F. Al-Saymari, A. P. Craig, and A. R. J. Marshall, "Resonant cavity enhanced photodiodes in the short-wave infrared for spectroscopic detection," IEEE Photonics Technol. Lett. **32**, 1369–1372 (2020).
17. S. Huang, G. Balakrishnan, and D. L. Huffaker, "Interfacial misfit array formation for gasb growth on gaas," J. Appl. Phys. **105**, 103104 (2009).
18. A. P. Craig, F. Al-Saymari, M. Jain, A. Bainbridge, G. R. Savich, T. Golding, A. Krier, G. W. Wicks, and A. R. Marshall, "Resonant cavity enhanced photodiodes on GaSb for the mid-wave infrared," Appl. Phys. Lett. **114**, 151107 (2019).
19. V. Letka, A. Bainbridge, A. P. Craig, F. Al-Saymari, and A. R. J. Marshall, "Resonant cavity-enhanced photodetector incorporating a type-II superlattice to extend mwir sensitivity," Opt. Express **27**, 23970–23980 (2019).
20. C. L. Canedy, W. W. Bewley, C. D. Merritt, C. S. Kim, M. Kim, M. V. Warren, E. M. Jackson, J. A. Nolde, C. A. Affouda, E. H. Aifer, I. Vurgaftman, and J. R. Meyer, "Resonant-cavity infrared detector with five-quantum-well absorber and 34% external quantum efficiency at 4μm," Opt. Express **27**, 3771–3781 (2019).
21. A. M. Green, D. G. Gevaux, C. Roberts, P. N. Stavrinou, and C. C. Phillips, "$\lambda \approx$ 3 μm InAs resonant-cavity-enhanced photodetector," Semicond. Sci. Technol. **18**, 964–967 (2003).

22. M. S. Ünlü and S. Strite, "Resonant cavity enhanced photonic devices," J. Appl. Phys. **78**, 607–639 (1995).
23. T. A. O'Loughlin, G. R. Savich, D. E. Sidor, B. T. Marozas, T. D. Golding, K. D. Jamison, L. Fredin, B. Fowler, W. Priyantha, and G. W. Wicks, "Mid-IR resonant cavity detectors," J. Vac. Sci. Technol., B **35**, 02B111 (2017).
24. V. Letka, A. P. Craig, A. Bainbridge, and A. R. J. Marshall, "A superlattice-based resonant cavity-enhanced photodetector operating in the long-wavelength infrared," Appl. Phys. Lett. **117**, 073503 (2020).
25. A. Bainbridge, A. P. Craig, F. Al-Saymari, A. Krier, and A. R. J. Marshall, "Resonant cavity–enhanced photodiodes for spectroscopy of C-H bonds," physica status solidi (a) **218**, 2100056 (2021).
26. A. Bainbridge, "Chirped RCE-PD linear array data," Lancaster Univ. (2021). 10.17635/lancaster/researchdata/495.